Comparison of main magnetic force computation methods for noise and vibration assessment in electrical machines

Raphaël PILE[13], Emile DEVILLERS[23], Jean LE BESNERAIS[3]
[1] Université de Toulouse, UPS, INSA, INP, ISAE, UT1, UTM, LAAS, ITAV, F-31077 Toulouse Cedex 4, France
[2] L2EP, Ecole Centrale de Lille, Villeneuve d'Ascq 59651, France
[3] EOMYS ENGINEERING, Lille-Hellemmes 59260, France (www.eomys.com)

In the vibro-acoustic analysis of electrical machines, the Maxwell Tensor in the air-gap is widely used to compute the magnetic forces applying on the stator. In this paper, the Maxwell magnetic forces experienced by each tooth are compared with different calculation methods such as the Virtual Work Principle based nodal forces (VWP) or the Maxwell Tensor magnetic pressure (MT) following the stator surface. Moreover, the paper focuses on a Surface Permanent Magnet Synchronous Machine (SPMSM). Firstly, the magnetic saturation in iron cores is neglected (linear B-H curve). The saturation effect will be considered in a second part. Homogeneous media are considered and all simulations are performed in 2D. The technique of equivalent force per tooth is justified by finding similar resultant force harmonics between VWP and MT in the linear case for the particular topology of this paper. The link between slot's magnetic flux and tangential force harmonics is also highlighted. The results of the saturated case are provided at the end of the paper.

***Index Terms*—Electromagnetic forces, Maxwell Tensor, Virtual Work Principle, Electrical Machines.**

I. Introduction

In electrical machines, the study of noise and vibrations due to magnetic forces first requires the accurate calculation of Maxwell stress distribution which depends on the time and space distribution of the magnetic flux density. Indeed a very small magnetic force harmonic can induce large acoustic noise and vibrations due to a resonance with a structural mode of the stator. The magnetic flux can be determined everywhere in the machine with a Finite Element Analysis (FEA), only in the air-gap and windings with semi-analytical methods such as Sub-Domain Model (SDM) [1], or only in the middle of the air-gap using the permeance magneto-motive force (PMMF).

In order to compute magnetic forces, a various range of methods can be found in the literature including: fictive magnetic currents and magnetic masses methods [2], energy methods [3], Maxwell Tensor (MT) methods [4], and Virtual Work Principle adapted to Finite Element (VWP) [5]. Then a compatible force computation method for the vibro-acoustic objectives must be chosen. As shown in the Table I, the two flagship methods are the VWP and the MT but the preference for one method or another is not clearly justified in the documentation and articles linked to these software (see column "Ref." of Table I).

The discussion of local magnetic pressure is still on going [24] [25] [26] and should be the aim of further work. The VWP is built to account for local magnetic behavior, while the Maxwell tensor gives the momentum flux across any surface, closed or not [24]. Historically the Maxwell Tensor has been used by electrical machine designers to accurately compute global quantities such as electromagnetic torque, which is the moment of the global magnetic force applied on a cylinder surrounding the rotor on its axis of rotation. Under the common form the MT cannot be rigorously related to a local magnetic pressure but it is often used in vibro-acoustic studies to obtain the local force distribution in the air gap which applies on the stator structure [8] [11] [15] [20]. However such a method can have strong limitations depending on the geometry as shown by [17].

Consequently, a common method to compute the magneto-mechanical excitations is to apply one integrated force per stator's tooth. It corresponds to the "Lumped Force Mapping" method proposed in [15]. A comparable integrated force per

TABLE I
MAGNETO-MECHANICAL COUPLING AMONG SOFTWARE FOR VIBRO-ACOUSTIC

EM Soft	Struct. Soft	Projection tool	Force calc.	Ref.
JMAG	LMS	LMS	VWP	[6] [7]
	NASTRAN	JMAG	MT	[8]
	ALTAIR	JMAG	MT	[8]
	ABAQUS	JMAG	MT	[8]
	JMAG	JMAG	VWP	[8]
FLUX	ANSYS	ANSYS	MT VWP	[9]
	LMS	LMS	VWP	[10]
	ALTAIR	FLUX	MT	[11]
	NASTRAN	FLUX	MT	[11]
	MATLAB	MATLAB	VWP	[11] [10]
COMSOL	COMSOL	COMSOL	MT	[12]
	MATLAB	MATLAB	MT VWP	[13] [14]
ANSYS	ANSYS	ANSYS	MT VWP	[15] [16]
	LMS	LMS	VWP	[17]
	NASTRAN	NASTRAN	MT	[15]
OPERA	OPERA	OPERA	MT VWP	[18]
FEMAG	FEMAG	FEMAG	MT	[19]
INFOLYTICA	NASTRAN	FSI Mapper	MT	[20]
	ACTRAN	FSI Mapper	MT	[20]
GETDP	GETDP	GETDP	MT VWP	[21] [22]
MANATEE	ALTAIR	MATLAB	MT VWP	[23]

tooth can be obtained using the VWP or the MT. For the VWP, the integrated force per tooth is directly the resultant of the nodal forces computed inside the tooth. For the MT, it is obtained by integrating the magnetic pressure in the air gap over a path "embracing/surrounding" the tooth. Thus, this paper proposes a comparison of the most common methods under local and integrated form with and without saturation effect. In order to perform the computation, MANATEE [23] is used because it is a privileged simulation framework for the vibro-acoustics study of electrical machines which can compute magnetic field with all these methods. Moreover it includes vibro-acoustic models showing good agreement with experiments.

The numerical values of the targeted Surface Permanent Magnet Synchronous Machine (SPMSM) machine with concentrated windings can be found in Table II. This validation case parameter is used all along this paper. This geometry which can be found in the article [27] is privileged because the long and thin stator's teeth are concentrating considerable radial and tangential efforts on teeth's tips such that the lumped force method is adapted. The geometry is presented on Fig. 4 and the flux lines in load case (no saturation) is illustrated on Fig. 1. A linear B-H curve and homogeneous media are considered for the whole machine. The geometry used in this paper has been successfully used with lumped force mapping by [28] with a MT applied in the air-gap.

TABLE II
INPUT PARAMETERS OF THE SPMSM 12S-10P MACHINE

Parameter	Value & Unit
Numerical	
Rotation speed N	400 [rpm]
Total time steps	160
Number of element (min/max)	[9142 ; 10798]
Number of nodes (min/max)	[4888 ; 5564]
Geometrical	
R_{ry}	11.9 [mm]
R_{rbo}	23.9 [mm]
R_m	26.8 [mm]
R_{sbo}	27.9 [mm]
R_{slot}	46.8 [mm]
R_{sy}	50.0 [mm]
Slot angular width	18 [deg]
Tooth angular width	12 [deg]
Depth	50 [mm]
Magnetic	
μ_0	4π1e-7 [$H.m^{-1}$]
μ_{stator}	1e5
μ_{magnet}	1.05
μ_{air}	1
Magnets B_{rm}	1.2 [T]
Windings	
Phase current RMS	10 [A]
Number of parallel circuits per phase	1
Number of turns per coil	34

II. NODAL FORCES WITH VIRTUAL WORK PRINCIPLE

A. Formulas & implementation

Let $\mathbf{H}$ be the magnetic field, $\mathbf{B}$ the magnetic flux density, H_i and B_i their respective components in cartesian frame. The nodal force expression proposed in [5] is based on an

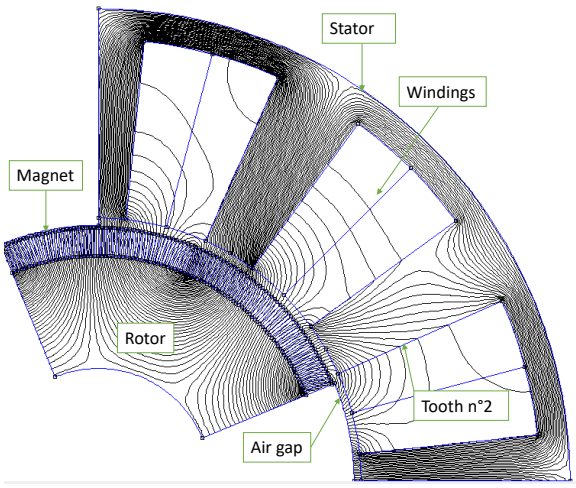

Fig. 1. Electrical motor flux map generated with FEMM [29] in loaded case

equivalence between the magnetic co-energy variation and the force applied on a solid determined by the domain Ω, such that the force amplitude in the direction $s \in \{\mathbf{x}, \mathbf{y}, \mathbf{z}\}$ is:

$$F_s = \frac{\partial}{\partial s} \int_\Omega \int_0^H \mathbf{B} \cdot d\mathbf{H} \; d\Omega \tag{1}$$

Applying this equation to a mesh element e:

$$F_s = \int_e \left(-\mathbf{B}^T \cdot \mathbb{J}^{-1} \cdot \frac{\partial \mathbb{J}}{\partial s} \cdot \mathbf{H} + \int_0^H \mathbf{B} \cdot d\mathbf{H} \; |\mathbb{J}^{-1}| \; \frac{\partial |\mathbb{J}|}{\partial s} \right) \tag{2}$$

with $\mathbb{J}$ the Jacobian matrix of the element e. The derivatives of $\mathbb{J}$ can be determined knowing the type of element (triangular, rectangular, quadrilateral, tetrahedron ...). With a linear case, the integrand of $\mathbf{B}$ can be simplified as follow:

$$\int_0^H \mathbf{B} \; . \; d\mathbf{H} = \int_0^H \mu \mathbf{H} \; . \; d\mathbf{H} = \frac{\mu}{2} |\mathbf{H}|^2 \tag{3}$$

with $\mathbf{H}$ constant in each element. Thus the natural way to implement the VWP algorithm is to loop on each element, compute the previous formulas and add the element contribution to its nodes. For a given node i:

$$F_s^i = \sum_{\forall e | i \in e} \int_e \left(-\mathbf{B}^T \cdot \mathbb{J}^{-1} \cdot \frac{\partial \mathbb{J}}{\partial s} \cdot \mathbf{H} + \frac{\mu}{2} |\mathbf{H}|^2 \; |\mathbb{J}^{-1}| \; \frac{\partial |\mathbb{J}|}{\partial s} \right) \tag{4}$$

B. Discussion

An overview of the magnetic force distribution according to Eq. (4) is presented on Fig. 2. A first observation is the concentration of nodal forces at the iron-air interface. This result is expected because of the linear homogeneous hypothesis media for the stator. In a linear electromagnetic media, the electromagnetic co-energy density is:

$$\psi(x, B(x)) = (1/\mu) \frac{|B|^2}{2} \tag{5}$$

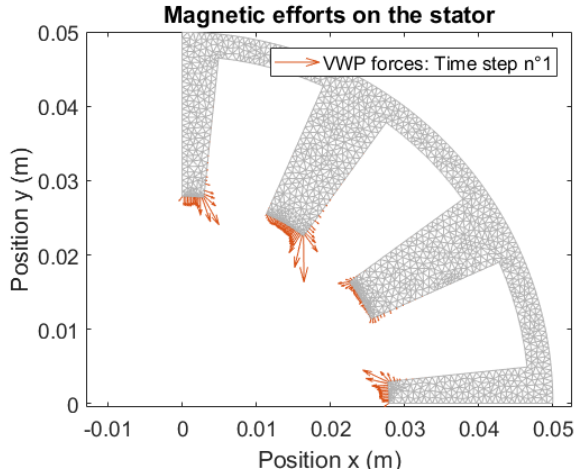

Fig. 2. Example of nodal magnetic force repartition using the VWP on the stator's mesh

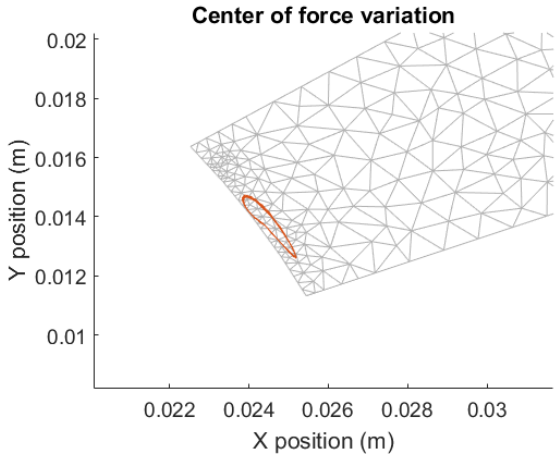

Fig. 3. Barycenter of forces trajectory during one revolution according to VWP nodal forces

Then the variation of energy density due to a virtual (or real) displacement $p : x \in \mathbb{R}^2 \rightarrow p(x) \in \mathbb{R}^2$ in case of weak-coupling ($B(p(x)) \approx B(x)$) is:

$$\psi(p(x), B(x)) - \psi(x, B(x)) \approx$$
$$[(1/\mu(p(x)) - 1/\mu(x)] \frac{|B(x)|^2}{2})$$

In the case of linear elasticity (small displacement) $\exists h \in \mathbb{R}^2$, $p(x) = x + h$ with $h \rightarrow 0$ such that :

$$\begin{aligned}\partial_p \psi(B) &= \lim_{h \to 0} \frac{\psi(x+h, B(x)) - \psi(x, B(x))}{h} \\ &= \lim_{h \to 0} \frac{1/\mu(x+h) - 1/\mu(x)}{h} \frac{|B(x)|^2}{2} \\ &= \nabla(1/\mu) \frac{|B(x)|^2}{2}\end{aligned}$$

The virtual work principle theorem (not the VWP method applied to FEA, see [30] for explanations) allows to identify the magnetic bulk force:

$$f_{mag} = \partial_p \psi(B) = \nabla(1/\mu) \frac{|B(x)|^2}{2} \tag{6}$$

Therefore, if the B-H curve is linear and μ constant in the stator, then we have $f_{mag} = 0$. This demonstration is inspired from the work of [31] who proposes to treat the interface problem with derivation in the distribution sense.

Another observation on the Fig. 2 is the concentration of the forces on the tip of each tooth. In order to investigate the accuracy of lumped force applied at the tooth tip, the Fig. 3 presents the displacement range of the barycenter of force (x_G, y_G) for one tooth over one revolution. For each tooth, the barycenter is computed by summing the contribution of all nodes i of the tooth:

$$\begin{pmatrix} x_G \\ y_G \end{pmatrix} = \frac{\sum_i \begin{pmatrix} F^i x_i \\ F^i y_i \end{pmatrix}}{\sum_i F^i} \tag{7}$$

with $F^i = \sqrt{(F_x^i)^2 + (F_y^i)^2}$ the L^2 norm of the force applied on the i^{th} node and (x_i, y_i) its Cartesian coordinates. On average, the center of force is close to the center of the tooth tip and under 2% of the total tooth height. The asymmetrical path and the difference between the average center and the tooth's tip center are explained by the asymmetrical average tangential forces between both edges, which produce the electromagnetic torque.

The linear hypothesis also means that both magnetic co-energy and magnetic energy are equivalent. However, this energetic symmetry is lost with non-linear media (by example for permanent magnets) resulting in different force distribution between co-energy and energy based formulations. This problem has been highlighted in [32], who proposed a solution based on a "reference" energy. A solution is also proposed in [33], by demonstrating generalized MT formulas and applying it on a FEA mesh with a virtual work principle formulation.

III. Maxwell Tensor Magnetic Pressure

A. Formulas & implementation

The Maxwell stress tensor $\mathbf{T}$ is commonly defined with the following component:

$$\mathbf{T}_{i,j} = B_i H_j - \frac{\mu}{2} \delta_{i,j} \sum_{k=1}^{n} |H_k|^2 \tag{8}$$

Defining a surface S around a volume V, such that the divergence theorem can be applied, with $\mathbf{n}$ the outer normal to S. Then the global force $\mathbf{F}$ applying on the volume V is:

$$\mathbf{F} = \iiint_V \nabla . \mathbf{T} dV = \oint_S \left((\mathbf{B}.\mathbf{n})\mathbf{H} - \frac{\mu}{2} |\mathbf{H}|^2 \mathbf{n} \right) dS \tag{9}$$

Applied to the ferromagnetic tooth surrounded by a dotted circular path on the Fig. 4, the force can be written under the form:

$$\begin{cases} F_n \approx \frac{1}{2} \int_S \frac{|B_n|^2}{\mu_0} - \mu_0 |H_t|^2 \, dS + \Gamma_n^{S \cap S'} \\ \qquad -\frac{1}{2} \int_{S'} \frac{|B_n|^2}{\mu} - \mu |H_t|^2 \, dS' \\ F_t \approx \int_S B_n H_t \, dS - \int_{S'} B_n H_t \, dS' + \Gamma_t^{S \cap S'} \end{cases} \tag{10}$$

with μ the magnetic permeability, μ_0 the void permeability, X_n and X_t the components of a vector field respectively

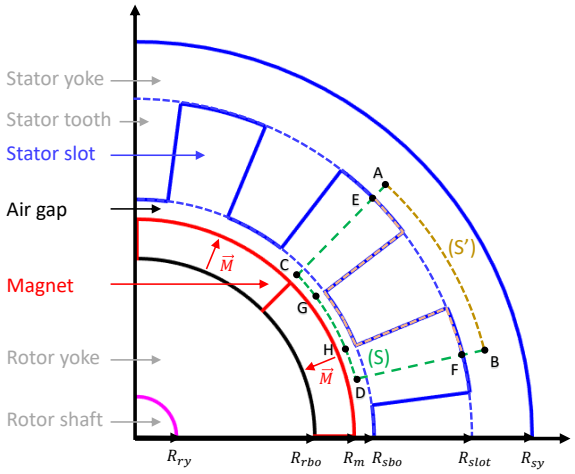

Fig. 4. Electrical motor geometry and parameters definition

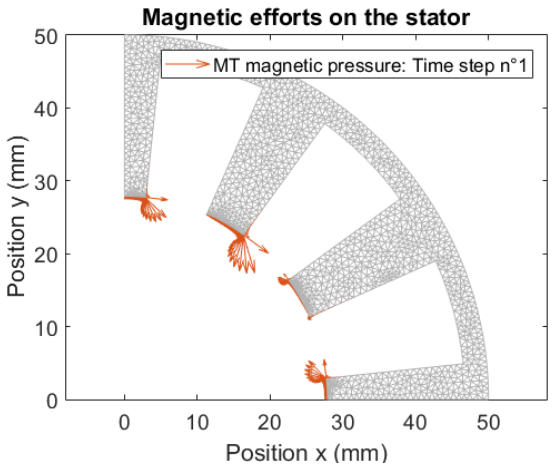

Fig. 5. Example of magnetic pressure repartition on the stator applying the MT along the stator inner surface

projected on $\mathbf{n}$ and $\mathbf{t}$ (local vectors attached to a surface) and $\Gamma^{S\cap S'}$ a gap term corresponding to the integration over the interface between the stator and the air. This form assumes the previous application of the divergence theorem is still valid when crossing a discontinuity of permeability which is the interface stator-air. It can be achieved using the mathematical distribution theory and an integration in the distribution sense.

However the common form used to compute forces applying on one tooth is:

$$\begin{cases} F_n \approx \frac{1}{2}\int_S \frac{|B_n|^2}{\mu_0} - \mu_0|H_t|^2 \; dS - \frac{1}{2}\int_{S'} \frac{|B_n|^2}{\mu} - \mu|H_t|^2 \; dS' \\ F_t \approx \int_S B_n H_t \; dS - \int_{S'} B_n H_t \; dS' \end{cases} \tag{11}$$

assuming $\Gamma^{S\cap S'}$ is null. Indeed, the numerical effect is negligible [34] when the integration surface cross the interface at points such as E and F on Fig. 4 where the magnetic flux in the air is low. Adding the hypothesis $\mu \gg \mu_0$, the force expression is commonly reduced to:

$$\begin{cases} F_n \approx \frac{1}{2}\int_S \frac{1}{\mu_0}|B_n|^2 - \mu_0|H_t|^2 \; dS \\ F_t \approx \int_S B_n H_t \; dS \end{cases} \tag{12}$$

In the vibro-acoustic context, simplifying assumptions are often added by neglecting the H_t terms which leads to:

$$\begin{cases} F_n \approx \frac{1}{2}\int_S \frac{1}{\mu_0}|B_n|^2 \; dS \\ F_t \approx 0 \end{cases} \tag{13}$$

These simplifications are coherent with analytical methods like PMMF which only compute radial magnetic field. It may be justified by the small effect of tangential lumped forces on the structural modes excitation [35]. To the authors knowledge, these assumptions have not been rigorously proved when considering local magnetic pressure.

B. Discussion

At this point, the integrand in Equation (12) could be identified as a "local magnetic pressure", as represented on the Fig. 5. Moreover, the previous VWP results, which show that the forces are indeed concentrated at the iron-air interface, corroborate the existence of such "local magnetic pressure".

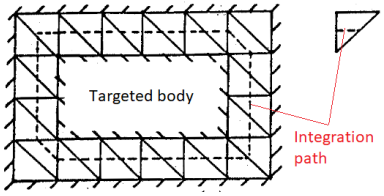

Fig. 6. Optimal contour for Maxwell-Tensor integration according to [38]

But as mentioned previously, it implies to arbitrary neglect some parts of the integration surface. A rigorous application of the MT is discussed in [26]. Even under the integrated form, there are many discussions about the choice of the integration surface, and its high influence on the vibro-acoustic results is a well-known problem [36] [37]. According to [38], the best choice with triangular finite elements is to cross the middle of the closest edges around the moving part, as illustrated with a closed path around a rectangular targeted body on Fig. 6. It agrees with [39] saying the integration surface should stay close to the targeted body. However, the construction of such a contour requires to find the correct edges and their neighborhoods. This operation increases the computation/implementation complexity especially with sharp or non-standard geometry and the precision gain might not be huge. It could explain why so many FEA software rely on the extrapolation of the middle air gap force to the lumped tooth model.

Regarding the semi-analytical methods, the magnetic field is not discretized such that the MT can be easily computed along any path. However, close to geometrical singularities (such as tooths corner) some unphysical Gibbs phenomenon can appear. To avoid this particular issue the MT is commonly computed at a certain distance of any interface (for example in the middle of the air-gap).

Concerning analytical methods (PMMF), only the normal magnetic field component in the air-gap is available, such that the MT computed in this context is equivalent to the Equation (13).

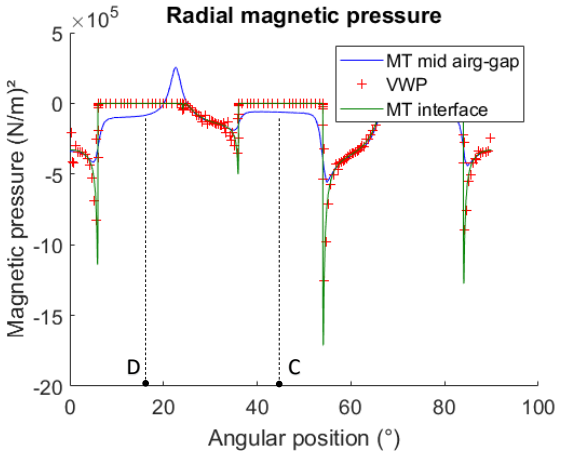

Fig. 7. Computing magnetic pressure in function of the angular position according to the VWP, the MT along the interface and the MT in the air-gap.

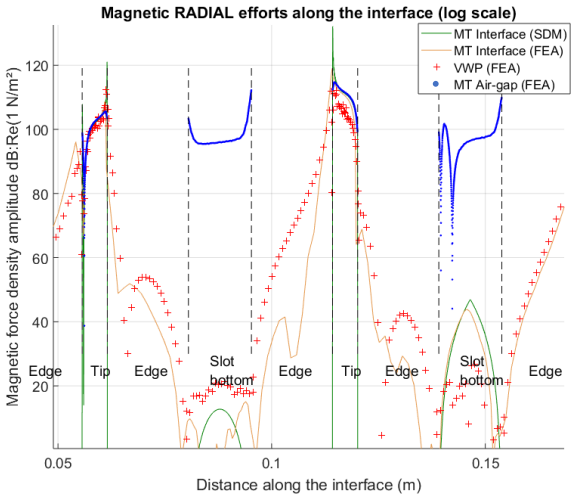

Fig. 8. Computing radial magnetic pressure along the interface according to the VWP, the MT along the interface and the MT in the air-gap.

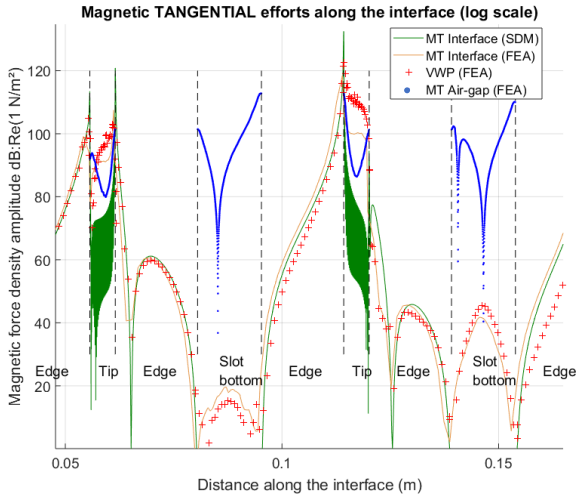

Fig. 9. Computing tangential magnetic pressure along the interface according to the VWP, the MT along the interface and the MT in the air-gap.

Although the local force density may be wrongly estimated, the MT ensures that integrated forces and torque are correctly conserved. It is coherent with the historical use of Maxwell Tensor by electrical machine designers to accurately compute torque. Moreover, [40] shows that approximation can be good enough to successfully predict the structural displacement using a MT local magnetic pressure with semi-analytical methods.

IV. Methods comparison: Linear Case

A. Local magnetic pressure

Fig. 7 compares local magnetic pressure computation according to different methods on the electrical machine of Fig. 1. At first only the radial component is studied since it is the main contributor to magnetic force. Three different methods are compared: the VWP computation based on FEA with FEMM [29], a "MT Interface" applied along the interface stator-air based on both SDM and FEA simulations, and a "MT Air gap" applied at constant radius in the middle of the air-gap based on FEA. Details about the application of these methods are provided in the Table III. The three different MT methods rely on the Equation (12) without the integrand. As observed on both Fig. 7 and 8, methods do not match each other on teeth tip, especially close to the tooth corners (i.e the points C and D). The magnetic pressure distribution highly depends on the choice of the distance between the integration path and the interface, and the choice of this distance is discussed afterwards.

Since the objective is the vibro-acoustic analysis, a logarithmic scale is more adapted because the acoustic amplitude A related to the magnetic force amplitude F is:

$$A \propto 20 \log \left(\frac{F}{F_{ref}} \right) \tag{14}$$

with F_{ref} a reference force. In this paper case $F_{ref} = 1$ [N] is used. Thus the magnetic forces are represented in logarithmic scale on Fig. 8 for radial component and on the Fig. 9 for the tangential component.

The dependence of the MT with the distance to the interface is even more clear in front of the slots. Initially, the MT is based on a volume, which is reduced to surface through a numerical approximation. This approximation is fulfilled in a linear case with a very high permeability for the stator. Then the tangential magnetic component $\mathbf{H}_t = 0$ and the normal flux $\mathbf{B}_n$ is nearly constant close to the interface, such that the MT tends to the following magnetic pressure P_{mag} approximation:

$$P_{mag} \approx \frac{1}{2\mu_0} |B_n|^2 \tag{15}$$

which is accurate for linear, planar surface with $\mu_{stator} \gg 1$. However, the geometric singularities (tooth's corners) does not satisfy these assumptions.

Since semi-analytical methods are used, the discretization effect is not studied here. An analysis of the mesh effect on the MT is proposed in [41] and further investigations about the accuracy of the MT depending on the integral surface are

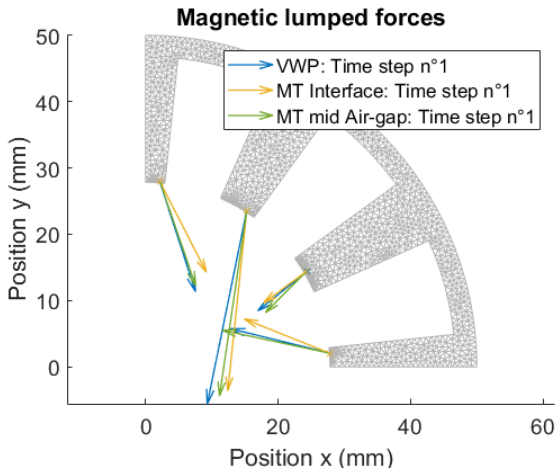

Fig. 10. Computing integrated tooth forces: Example of lumped forces amplitude and direction per teeth according to different methods.

available in [42]. Although the local magnetic pressure may be wrongly estimated, this method ensures that integrated forces and torque are correctly conserved as shown in the following sections.

B. Lumped force mapping

In this section, the previous magnetic pressures are integrated and compared for a vibro-acoustic purpose. First an example of the results with these "lumped forces" is presented on Fig. 10.

To better understanding the notion of "magnetic momentum" represented by the MT, additional versions of the MT lumped forces are computed in the following. The set of methods is summarized in the Table III.

TABLE III
SET OF FORCE METHODS USED FOR THE LUMPED FORCE COMPARISON

Name	Force method	Magnetic field method
MT Air-gap	Maxwell Tensor computed according to Equation (12) along the green curve between point D & C on Fig. 4	SDM with MANATEE or FEA with FEMM
MT Interface	Maxwell Tensor computed according to Equation (12) along the beige curve between point F & E on Fig. 4	SDM with MANATEE or FEA with FEMM
VWP	Virtual work principle applied to Finite Element according to Equation (4)	FEA with FEMM
MT-radial	Maxwell Tensor computed according to Equation (13) along the green curve between point D & C on Fig. 4	SDM with MANATEE
MT Tooth Tip	Maxwell Tensor computed according to Equation (12) along the green curve between point H & G on Fig. 4	SDM with MANATEE

The first global value which can be numerically compared is the magnetic torque applying on the stator in Table IV.

TABLE IV
GLOBAL TORQUE ON THE MACHINE OF TABLE II WITH A LINEAR B-H CURVE SIMULATION

Average torque	Value $[N.m^{-1}]$
MT Air-gap (FEA)	-8.3
MT Interface (FEA)	-8.2
VWP (FEA)	-9.2
MT Radial (SDM)	0
MT Tooth Tip (SDM)	-5.0
MT Air-gap (SDM)	-8.1
MT Interface (SDM)	-9.9

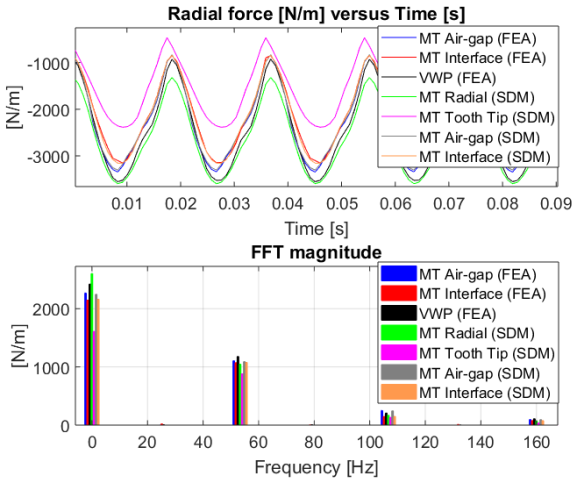

Fig. 11. Radial lumped force during one revolution and its FFT according to different methods with a linear B-H curve

For each tooth, the integrated forces computed according to the different methods are represented on Fig. 11 for the radial component, on Fig. 12 for the tangential component and on Fig. 14 for the electromagnetic torque. The resulting frequencies f_n of the force harmonics are even multiple of the fundamental frequency f_s, such as :

$$f_n = 2nf_s = (2n)p\frac{N}{60} \approx (53.33)n\ [H_z]\ ,\ \forall n \in \mathbb{N} \quad (16)$$

This result is observed for all three methods on both figures after performing a Fast Fourier Transform (FFT) on the discrete temporal signals. The three methods give the same frequency content, only the magnitude of the harmonics differ. The value of A according to (14) differs of less than 3% between the different methods for the radial component of Fig. 11.

Moreover, effect of numerical noise can be observed on the Fig. 13 for VWP (and to a lesser extent for the MT FEMM) through small non-physical harmonics. This noise is due to mesh discretization. Besides only three out of five methods really account for the tangential direction contribution: VWP, "MT Air-gap" and "MT Interface". Indeed only the MT methods which take into account the slot magnetic flux can capture correctly the tangential lumped force. Thus "MT-radial" and "MT Tooth Tip" are not appropriate to study the tangential excitations. Moreover, neglecting the tangential magnetic flux (with the "MT-radial") leads to overestimate the radial lumped force.

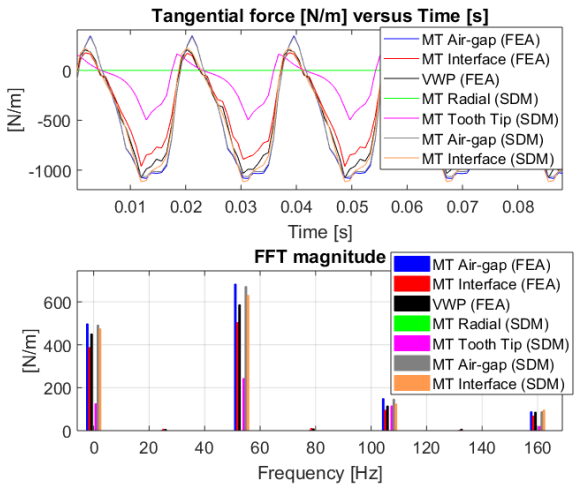

Fig. 12. Tangential lumped force during one revolution and its FFT according to different methods with a linear B-H curve

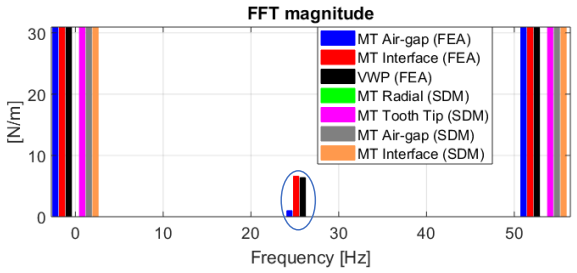

Fig. 13. Integrated tooth forces: Zoom on the FEA noise on the lumped tangential forces

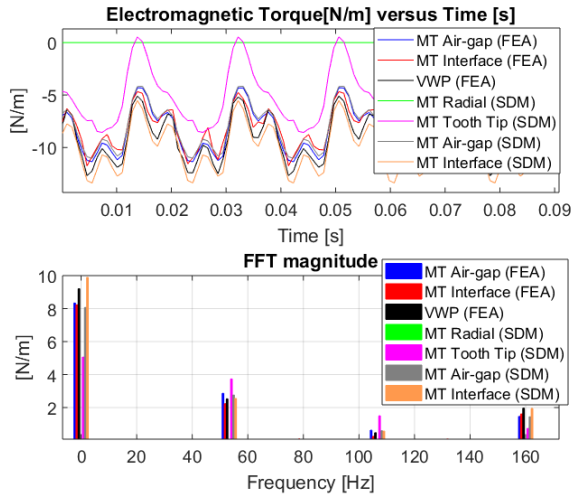

Fig. 14. Electromagnetic torque during one revolution and its FFT according to different methods with a linear B-H curve

Since the components harmonics and amplitudes are very close, the following methods are nearly equivalent from a vibro-acoustic point of view: VWP, MT Interface, MT Air-gap and MT FEMM. Then the lumped force mapping can be used for vibro-acoustic prediction with similar tooth geometry. For example, [28] presented a successful prediction of the noise

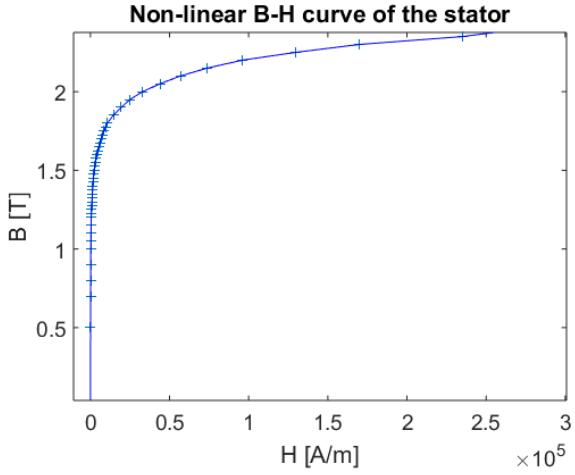

Fig. 15. Non-linear B-H curve used for the stator in FEMM

with lumped force mapping using the "MT Air-gap". The case of Table II has a good agreement between linear and non-linear simulations. In order to start a study about the saturation effect, the following section proposes to keep the same geometry with higher injection currents and higher remanent magnetization.

C. Saturation effect

In this section, the simulation is now performed with the same geometry but the injected current and the remanent magnetization of the rotor's magnet are both increased. The modified magnetic and windings parameters can be found in the Table V. The FEMM simulation is performed with a non-linear B-H curve presented on the Fig. 15, such that the saturation can be computed. The most visible effect of the saturation is the recoil of forces inside the stator volume as shown on the Fig. 16. Indeed, the saturation results in a drop of the local magnetic permeability inside the material. It creates a gradient of permeability across the media such that a magnetic bulk force (orthogonal to iso-permeability lines) is obtained according to the Eq. (6). Thus magnetic forces are not completely concentrated at the interface unlike the linear case. Though the barycenter of forces on Fig. 17 is pushed back into the stator compared to the Fig. 3, the highest point is approximately at 22% of the total tooth height, such that the application of the force at the tooth starts to be questionable. Moreover the "MT Interface" approximation of the barycenter position is distort by the presence of bulk forces.

TABLE V
MODIFIED PARAMETERS OF THE MACHINE WITH SATURATION

New Parameter	Value & Unit
Magnets B_{rm}	1.4 [T]
Phase current RMS	25 [A]

The SDM simulation is not accounting for the saturation effect on the magnetic flux, resulting in differences presented on the Fig. 18: the temporal harmonic content on the flux is the same but the amplitude differs on the fundamental and the first harmonic. Indeed, the saturation is flattening the spatial

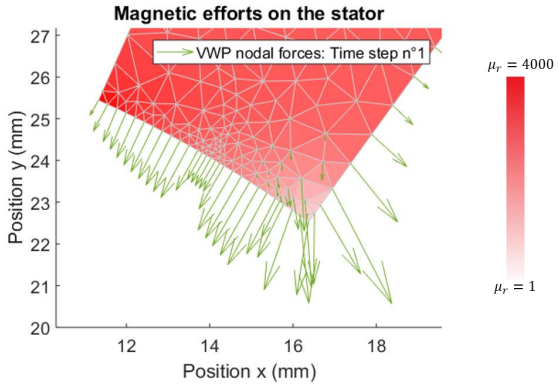

Fig. 16. Apparition of bulk force in saturated conditions according to VWP

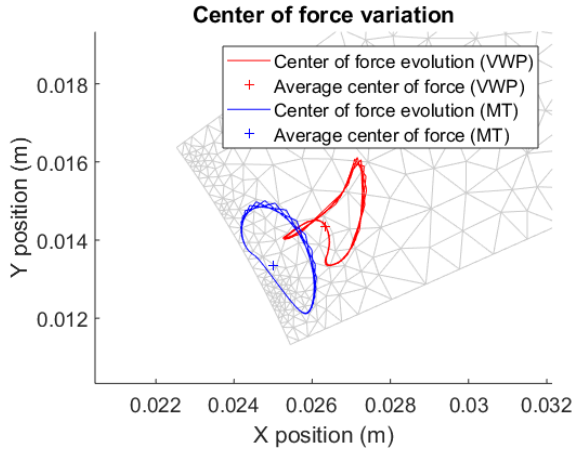

Fig. 17. Barycenter of forces trajectory during one revolution (simulation with saturation)

TABLE VI
GLOBAL TORQUE ON THE MACHINE WITH SATURATION

Average torque	**Value** $[N.m^{-1}]$
MT Air-gap (FEA)	-20.8
MT Interface (FEA)	-17.4
VWP (FEA)	-23.8
MT Radial (SDM)	0
MT Tooth Tip (SDM)	-14.8
MT Air-gap (SDM)	-23.5
MT Interface (SDM)	-28.8

distribution of magnetic flux such that the first harmonics are lower than with SDM.

With the new conditions, the Fig. 19-20 respectively show the radial and tangential lumped forces and Fig. 21 the global torque. It is observable that the saturation effect is not introducing new temporal harmonics but the effect on the amplitude of the integrated quantities become obvious. In particular, the saturation is reducing the amplitude of the magnetic field in the air-gap and thus the average value of the electromagnetic torque (see Table VI). Since the SDM simulation is not accounting for the saturation, the torque (or tangential force) amplitude of the "MT Air-gap" and "MT Interface" are higher than the "MT FEMM" or the "VWP".

In the end, the methods are compared in terms of amplitude

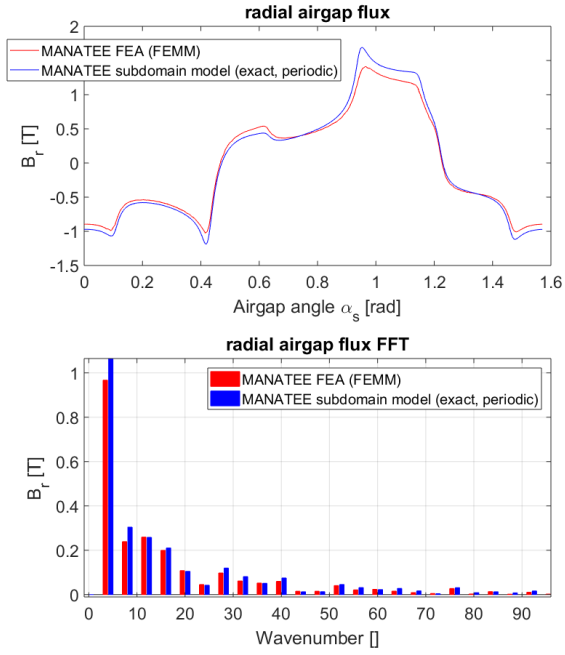

Fig. 18. Comparison between FEA with saturation and SDM

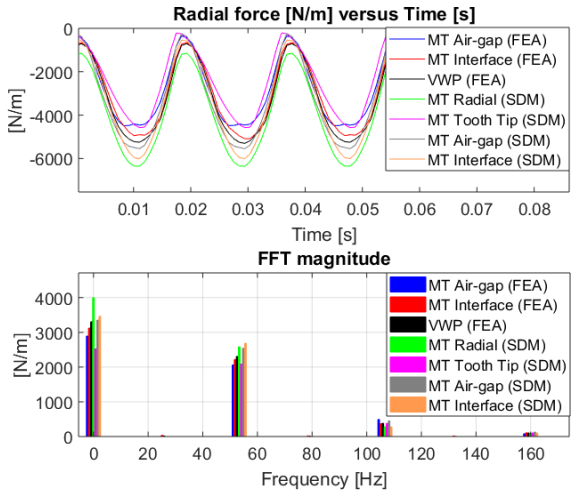

Fig. 19. Radial lumped force during one revolution and its FFT according to different methods with a non linear B-H curve

TABLE VII
MAXIMUM AMPLITUDE DIFFERENCES BETWEEN FORCE CALCULATION METHOD (IN DB SCALE)

Force	**Maximum difference**	
	Linear	**Saturated**
Radial	2.4 dB	3.6 dB
Tangential	4.8 dB	10.8 dB
Torque	4 dB	10.0 dB

differences in the logarithmic scale in the Table VII. Because of the lack of physics, the "MT Tooth Tip (SDM)" and the "MT Radial (SDM)" have been ignored to compute the values in the Table VII.

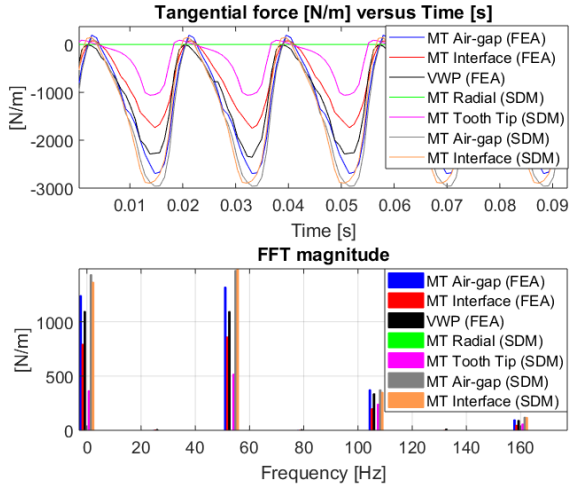

Fig. 20. Tangential lumped force during one revolution and its FFT according to different methods with a non linear B-H curve

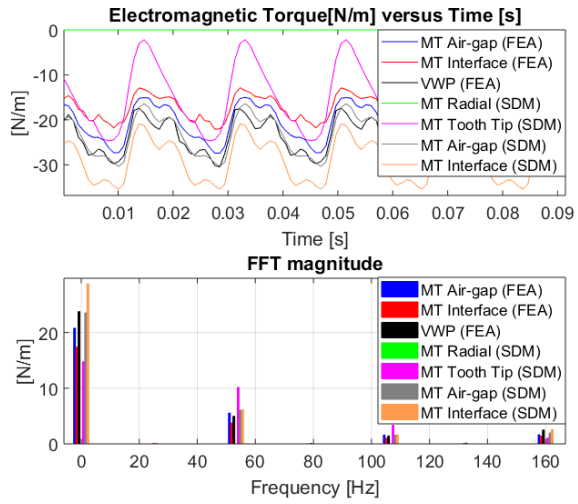

Fig. 21. Electromagnetic torque during one revolution and its FFT according to different methods with a non-linear B-H curve

V. Conclusion

This paper proposes a comparison between different magnetic forces computation methods for vibro-acoustic purpose. The local magnetic pressure differs between methods (see section IV-A) and the MT methods computed in the air-gap do not properly compute the local magnetic pressure especially at the bottom of the slot. Then it is more convenient to compare methods under integrated form. For this type of slot geometry, this paper shows that lumped force mapping applied at the center of the tooth tip for vibro-acoustic does not really depend on the method used to compute magnetic forces if the method is correctly conserving global quantities (especially torque) and if it is integrated between two slot opening. Moreover the last part of the paper shows that the assumptions of the lumped force at tooth tip method are weakened by the saturation. Knowing that some geometries are more sensitive to saturation, there is certainly a link between the geometry and the validity of the lumped force methods. The characterization of this sensitivity is the matter of further work.

Therefore the advantages of using the Maxwell Tensor in the air gap with lumping force mapping (as it is done in MANATEE software) are: the compatibility with any electromagnetic fields computations (SDM, FEM, PMMF ...), it does not require any knowledge on the stator geometry (at least for standard geometries), it is very light in term of computational cost and is as accurate as nodal methods.

The authors goal is to provide in a later paper further investigations on a comparison in the electrical machine noise context between nodal forces projection (which should be more accurate) and simplified methods such as lumped force mapping.

Acknowledgment

The authors would like to thank Olivier Barré for sharing his knowledge on magneto-mechanical physics.

References

[1] E. Devillers, J. Le Besnerais, T. Lubin, M. Hecquet, and J.-P. Lecointe, "A review of subdomain modeling techniques in electrical machines: performances and applications," in *Electrical Machines (ICEM), 2016 XXII International Conference on*. IEEE, 2016, pp. 86–92. [Online]. Available: http://ieeexplore.ieee.org/document/7732510/

[2] O. Barré, "Contribution à l'étude des formulations de calcul de la force magnétique en magnétostatique, approche numérique et validation expérimentale," Ph.D. dissertation, Centrale Lille, 2003. [Online]. Available: https://tel.archives-ouvertes.fr/tel-00005921/document

[3] J. Kirtley, James L., *Class Notes 1: Electromagnetic Forces*, 2005. [Online]. Available: http://web.mit.edu/course/6/6.685/www/chapter1.pdf

[4] K. J. Meessen, J. J. H. Paulides, and E. A. Lomonova, "Force calculations in 3-D cylindrical structures using fourier analysis and the maxwell stress tensor," *IEEE Transactions on Magnetics*, vol. 49, no. 1, pp. 536–545, 2013. [Online]. Available: http://ieeexplore.ieee.org/document/6228537/

[5] J. L. Coulomb and G. Meunier, "Finite element implementation of virtual work principle for magnetic or electric force and torque computation," *IEEE Transactions on Magnetics*, vol. 20, no. 5, pp. 1894–1896, 1984. [Online]. Available: http://ieeexplore.ieee.org/document/1063232/

[6] G. Kumar, "Noise prediction for electric motors by coupling electromagnetic and vibroacoustic simulation tools," in *Proceedings of NAFEMS conference*, 2014. [Online]. Available: https://www.nafems.org/.../uk_2014_mpconf/abstracts/041_kumar.pdf

[7] F. Chauvicourt, C. Faria, A. Dziechciarz, and C. Martis, "Influence of rotor geometry on nvh behavior of synchronous reluctance machine," in *Ecological Vehicles and Renewable Energies (EVER), 2015 Tenth International Conference on*. IEEE, 2015, pp. 1–6. [Online]. Available: http://ieeexplore.ieee.org/document/7112973/

[8] T. Hattori, "Starting with vibration noise analyses," p. Vol. 1, 2014. [Online]. Available: https://www.jmag-international.com/newsletter/201401/05.html

[9] F. Z. Hamza ENNASSIRI, "Magneto-vibro-acoustic analysis linking flux to ansys mechanical," pp. CEDRAT News – N 6, 2016. [Online]. Available: http://www.cedrat.com/Publications/

[10] J. Hallal, "Etudes des vibrations d'origine électromagnétique d'une machine électrique: conception optimisée et variabilité du comportement vibratoire," Ph.D. dissertation, Compiègne, 2014. [Online]. Available: www.theses.fr/2014COMP1900/abes

[11] P. Lombard, "Summary vibro-acoustic coupling," 2017.

[12] V. Wilow, "Electromagnetical model of an induction motor in comsol multiphysics," 2014. [Online]. Available: http://www.diva-portal.se/smash/get/diva2:790873/FULLTEXT01.pdf

[13] M. K. Nguyen, "Masters thesis : Predicting electromagnetic noise in induction motors," 2014. [Online]. Available: http://www.diva-portal.se/smash/get/diva2:742541/FULLTEXT01.pdf

[14] M. Nguyen, R. Haettel, and A. Daneryd, "Prediction of noise generated by electromagnetic forces in induction motors," 2014. [Online]. Available: https://www.comsol.nl/paper/download/199305/haettel_paper.pdf

[15] M. Solveson, C. Rathod, M. Hebbes, G. Verma, and T. Sambharam, "Electromagnetic Force Coupling in Electric Machines," ANSYS Inc, Tech. Rep., 2011. [Online]. Available: http://resource.ansys.com
[16] X. Ge, "Simulation of vibrations in electrical machines for hybrid-electric vehicles," Ph.D. dissertation, MS Thesis, Department of Applied Mechanics, Chalmers University of Technology, Göteborg (Sweden), 2014. [Online]. Available: http://publications.lib.chalmers.se/records/fulltext/199927/199927.pdf
[17] F. Lin, S. Zuo, W. Deng, and S. Wu, "Modeling and analysis of electromagnetic force, vibration, and noise in permanent-magnet synchronous motor considering current harmonics," *IEEE Transactions on Industrial Electronics*, vol. 63, no. 12, pp. 7455–7466, 2016. [Online]. Available: http://ieeexplore.ieee.org/document/7518596/
[18] M. U. Guide, "Cobham technical services, 24 bankside, kidlington."
[19] K. Reichert, "A simplified approach to permanent magnet and reluctance motor characteristics determination by finite-element methods," *COMPEL-The international journal for computation and mathematics in electrical and electronic engineering*, vol. 25, no. 2, pp. 368–378, 2006.
[20] N. Wirth, "Simulation of flow and electro-magnetic induced vibrations - mapping procedures for nvh analyses," 2016.
[21] M. Rossi and J. Le Besnerais, "Vibration reduction of inductors under magnetostrictive and maxwell forces excitation," *IEEE Transactions on Magnetics*, vol. 51, no. 12, pp. 1–6, 2015. [Online]. Available: http://ieeexplore.ieee.org/document/7208876/
[22] P. Dular and C. Geuzaine, "Getdp reference manual: the documentation for getdp, a general environment for the treatment of discrete problems," *University of Liège*, 2013. [Online]. Available: http://getdp.info/
[23] J. Le Besnerais, "Fast prediction of variable-speed acoustic noise and vibrations due to magnetic forces in electrical machines," in *ICEM International Conference on Electrical Machines*, 2016. [Online]. Available: http://ieeexplore.ieee.org/document/7732836/
[24] A. Bossavit, "A note on the uniqueness of the poynting vector and of the maxwell tensor," *International Journal of Numerical Modelling: Electronic Networks, Devices and Fields*, 2016. [Online]. Available: http://onlinelibrary.wiley.com/doi/10.1002/jnm.2214/full
[25] A. Bermúdez, A. Rodríguez, and I. Villar, "Extended formulas to compute resultant and contact electromagnetic force and torque from maxwell stress tensors," *IEEE Transactions on Magnetics*, vol. 53, no. 4, pp. 1–9, 2017. [Online]. Available: http://ieeexplore.ieee.org/document/7762235/
[26] F. Henrotte and K. Hameyer, "A theory for electromagnetic force formulas in continuous media," *IEEE Transactions on Magnetics*, vol. 43, no. 4, pp. 1445–1448, 2007. [Online]. Available: http://ieeexplore.ieee.org/document/4137733/
[27] Z. Zhu, L. Wu, and Z. Xia, "An accurate subdomain model for magnetic field computation in slotted surface-mounted permanent-magnet machines," *IEEE Transactions on Magnetics*, vol. 46, no. 4, pp. 1100–1115, 2010.
[28] A. Saito, M. Kuroishi, and H. Nakai, "Vibration prediction method of electric machines by using experimental transfer function and magnetostatic finite element analysis," *Journal of Physics: Conference Series*, vol. 744, no. 1, p. 012088, 2016. [Online]. Available: http://stacks.iop.org/1742-6596/744/i=1/a=012088
[29] D. Meeker, "Finite element method magnetics," *FEMM*, vol. 4, p. 32, 2010.
[30] J. Coulomb, G. Meunier, and J. Sabonnadiere, "An original stationary method using local jacobian derivative for direct finite element computation of electromagnetic force, torque and stiffness," *Journal of Magnetism and magnetic Materials*, vol. 26, no. 1-3, pp. 337–339, 1982.
[31] A. Bossavit, "Bulk forces and interface forces in assemblies of magnetized pieces of matter," *IEEE Transactions on Magnetics*, vol. 52, no. 3, pp. 1–4, 2016. [Online]. Available: http://ieeexplore.ieee.org/abstract/document/7286815/
[32] L. De Medeiros, G. Reyne, and G. Meunier, "Comparison of global force calculations on permanent magnets," *IEEE Transactions on magnetics*, vol. 34, no. 5, pp. 3560–3563, 1998. [Online]. Available: http://ieeexplore.ieee.org/document/717840/
[33] F. Henrotte and K. Hameyer, "Computation of electromagnetic force densities: Maxwell stress tensor vs. virtual work principle," *Journal of Computational and Applied Mathematics*, vol. 168, no. 1-2, pp. 235–243, 2004.
[34] J. Roivainen *et al.*, "Unit-wave response-based modeling of electromechanical noise and vibration of electrical machines," 2009. [Online]. Available: http://lib.tkk.fi/Diss/2009/isbn9789512299119/
[35] E. Devillers, M. Hecquet, J. Le Besnerais, and M. Régniez, "Tangential effects on magnetic vibrations and acoustic noise of induction machines using subdomain method and electromagnetic vibration synthesis," in *Electric Machines and Drives Conference (IEMDC), 2017 IEEE International*. IEEE, 2017, pp. 1–8. [Online]. Available: http://ieeexplore.ieee.org/document/8002072/
[36] J. Hallal, F. Druesne, and V. Lanfranchi, "Study of electromagnetic forces computation methods for machine vibration estimation," *ISEF2013, Ohrid, Macedonia*, 2013.
[37] M. Krishnamurthy and B. Fahimi, "Qualitative analysis of force distribution in a 3-phase permanent magnet synchronous machine," in *Electric Machines and Drives Conference, 2009. IEMDC'09. IEEE International*. IEEE, 2009, pp. 1105–1112. [Online]. Available: http://ieeexplore.ieee.org/document/5075342/
[38] J. Coulomb, "A methodology for the determination of global electromechanical quantities from a finite element analysis and its application to the evaluation of magnetic forces, torques and stiffness," *IEEE Transactions on Magnetics*, vol. 19, no. 6, pp. 2514–2519, Nov 1983. [Online]. Available: http://ieeexplore.ieee.org/document/1062812/
[39] M. Boesing, T. Schoenen, and K. A. Kasper, "Vibration Synthesis for Electrical Machines Based on Force Response Superposition," *IEEE Transactions on Magnetics*, vol. 46, no. 8, pp. 2986–2989, aug 2010. [Online]. Available: http://ieeexplore.ieee.org/document/5513016/
[40] H. Hu, J. Zhao, X. Liu, Y. Guo, and J. Zhu, "No-load magnetic field and cogging force calculation in linear permanent-magnet synchronous machines with semiclosed slots," *IEEE Transactions on Industrial Electronics*, vol. 64, no. 7, pp. 5564–5575, 2017. [Online]. Available: http://ieeexplore.ieee.org/document/7801011/
[41] A. Wignall, A. Gilbert, and S. Yang, "Calculation of forces on magnetised ferrous cores using the maxwell stress method," *IEEE Transactions on Magnetics*, vol. 24, no. 1, pp. 459–462, 1988. [Online]. Available: http://ieeexplore.ieee.org/document/43956/
[42] J. Mizia, K. Adamiak, A. Eastham, and G. Dawson, "Finite element force calculation: comparison of methods for electric machines," *IEEE Transactions on Magnetics*, vol. 24, no. 1, pp. 447–450, 1988. [Online]. Available: http://ieeexplore.ieee.org/document/43953/

Raphaël PILE is currently doing a Master thesis internship at EOMYS ENGINEERING (Lille, France) in order to graduate from both Universit PAUL SABATIER (Toulouse) M.Sc. in Fundamental and Applied Mathematics, and ISAE-SUPAERO (Toulouse) M.Sc. in Aeronautical Engineering.

Emile DEVILLERS is currently doing an industrial PhD thesis at EOMYS ENGINEERING (Lille, France) and L2EP laboratory of the Ecole Centrale de Lille, North of France. His research interests are the modeling of noise and vibrations in electrical machines due to magnetic forces for reduction purposes. He obtained a M.Sc. specialized in Energy Systems in 2015 from the Grenoble Institute of Technology, France.

Jean LE BESNERAIS currently works in EOMYS ENGINEERING as an R&D engineer on the analysis and reduction of acoustic noise and vibrations in electrical systems. He made an industrial PhD thesis in Electrical Engineering at the L2EP laboratory (Lille, France), on the reduction of electromagnetic noise and vibrations in traction induction machines with ALSTOM Transport. In 2013, he founded EOMYS ENGINEERING, a company providing applied research and development services including modeling and simulation, scientific software development and experimental measurements.